Available online at www.sciencedirect.com
ScienceDirect
Journal of Sound and Vibration 309 (2008) 569–587
JOURNAL OF SOUND AND VIBRATION
www.elsevier.com/locate/jsvi

Karhunen–Loeve analysis and order reduction of the transient dynamics of linear coupled oscillators with strongly nonlinear end attachments

Xianghong Ma[a,*], Alexander F. Vakakis[b,c,d], Lawrence A. Bergman[e]

[a]*School of Engineering and Applied Science, Aston University, Birmingham B4 7ET, UK*
[b]*Division of Mechanics, National Technical University of Athens, Greece*
[c]*Department of Mechanical and Industrial Engineering (adjunct), University of Illinois at Urbana-Champaign, IL, USA*
[d]*Department of Aerospace Engineering (adjunct), University of Illinois at Urbana-Champaign, IL, USA*
[e]*Department of Aerospace Engineering, University of Illinois at Urbana-Champaign, IL, USA*

Received 1 June 2007; received in revised form 24 July 2007; accepted 24 July 2007
Available online 17 September 2007

Abstract

The Karhunen–Loeve (K–L) decomposition method has become a popular technique to create low-dimensional, reduced-order models of dynamical systems. In this paper this technique is applied to a multi-degree-of-freedom chain of linear coupled oscillators with a strongly nonlinear (nonlinearizable), lightweight end attachment. By performing K–L decomposition we show that the lightweight nonlinear attachment (possessing 0.5% of the total mass of the chain) can affect the global dynamics of the linear chain, exhibiting nonlinear energy-pumping phenomena; that is, irreversible passive targeted energy transfers from the linear chain to the nonlinear end attachment, where this energy is locally confined and dissipated without 'spreading back' to the primary system. It is shown that the occurrence of energy pumping can be identified by studying the dominant K–L modes of the dynamics, as well as, the energy distribution among them. Moreover, by comparing the action of the strongly nonlinear attachment to the classical linear vibration absorber, we show robustness of passive nonlinear energy absorption over wide parameter ranges. On the other hand, the case-sensitive nature of K–L-based reduced-order models has always been a constraint for K–L decomposition, since one cannot quantify *a priori* the error bound of such low-dimensional reduced-order models when different initial conditions are applied to the system. To alleviate this constraint, the paper proposes a multiple correlation coefficient (MCC) as a quantitative measure to effectively assess the applicability of a K–L-based reduced-order model derived for a specific set of initial conditions to a small neighborhood of initial conditions containing that initial state. The derived reduced-order models are validated through reconstruction of the system responses and comparisons to direct numerical integrations.

Abbreviations: 2dof NES, two-dof NES; dof NES, degree-of-freedom; EMD, energy measure of dissipation; K–L, Karhunen–Loeve; MCC, multiple correlation coefficient; NES, nonlinear energy sink; sdof NES, single-dof NES; WT, wavelet transform

*Corresponding author. Tel.: +44 121 204 3592.
E-mail addresses: x.ma@Aston.ac.uk (X. Ma), vakakis@central.ntua.gr, avakakis@uiuc.edu (A.F. Vakakis), lbergman@uiuc.edu (L.A. Bergman).

0022-460X/$ - see front matter © 2007 Elsevier Ltd. All rights reserved.
doi:10.1016/j.jsv.2007.07.053

Nomenclature

C	stiffness of the nonlinear spring
$\mathbf{C}$	damping matrix
d	coupling stiffness of the chain
E_{input}	input energy
H	energy dissipation measure—EMD
$\mathbf{K}$	stiffness matrix
$\mathbf{M}$	mass matrix
$\mathbf{N}(\ )$	vector of nonlinear terms
t	time variable
$\mathbf{U}$	matrix of the first 4 K–L modes
v	displacement of the nonlinear attachment
$\underline{x}$	vector in R^N
$\mathbf{X}(t)$	displacement vector of the reduced-order model
$y_0, y_1, \ldots y_9$	displacements of the particles of the chain
$\mathbf{Y}(t)$	displacement vector of the full-order model
ε	small parameter
λ	damping factor
$\hat{\lambda}$	K–L eigenvalue
ϕ	K–L mode shape
ω_0	normalized grounding stiffness
$[]^{\mathrm{T}}$	transpose of a vector

1. Introduction

The K–L decomposition or proper orthogonal decomposition (POD) is a method of representing a stochastic system in terms of a minimum number of degrees-of-freedom. It provides a way to extract spatial coherent structures (POMs) from a set of time series measurements. The origin of the method dates back to 1940s and 1950s when Karhunen [1] and Loeve [2] laid the theoretical foundation for the analysis. This method has been applied extensively in various research fields, including fluid mechanics [3–5], fluid–structure interaction problems [6], and chemical reaction–diffusion dynamics [7,8]. In fluid dynamics, Lumley [9–11] suggested that the method can provide a concrete mathematical framework to extract coherent structures, studying chaotic behavior due to turbulence in dynamical fluid and meteorological phenomena. Sirovich [3,12] further applied the method to vector-valued data, and extended the application of the method from one-dimensional to three-dimensional flow problems. In Ref. [12] the K–L decomposition method was applied to study chaotic behavior of turbulent flows. K–L modes are used to create low-order dynamical models and the energy of the corresponding modes are used to provide a measure of the dimensionality of the system under consideration. Applications of K–L decomposition to structural dynamics can be found in various studies by Cusumano et al. [13], Georgiou and co-workers [14,15], Azeez and Vakakis [16], Ma and Vakakis [17–20], Feeny and Kappagantu [21], Kerschen and Golinval [22–24], and most recently by Trindade et al. [25], Glosmann and Kreuzer [26], Lin et al. [27] and Iemma et al. [28].

K–L decomposition has been applied to linear as well as nonlinear dynamical problems to construct low-dimensional models that capture accurately the dynamics. The orthogonal eigenfunctions (POMs or K–L modes) derived by processing experimental or numerical time series measured at different positions throughout the system can be proven to optimal in the linear case, in the sense that fewer K–L modes are needed to account for the same amount of vibration energy, compared to modes resulting from application of standard Galerkin or Rayleigh–Ritz procedures [29].

A well-know restriction of K–L decomposition, however, is that it is case-specific. That is, the set of K–L modes and the associated low-dimensional model derived for a specific dynamic application, hold only for that application, in the sense that they are expected to vary if the initial or forcing conditions of the system change. It follows that a K–L-based reduced-order model constructed under a specific set of initial and forcing conditions is not necessarily suitable for use in other conditions, although a small neighboring region of initial and forcing conditions is generally considered as acceptable. To the authors' knowledge there is no method available to quantify the error that results when a set of K–L modes derived for a specific set of initial and forcing conditions is used to reduce the dynamics of the system subject to 'neighboring' initial and forcing conditions. In this paper we propose to use a multiple correlation coefficient (MCC) as the quantitative

measurement to assess the range of regions of validity of a set of specific K–L modes to the dynamics of the system under different initial or forcing conditions.

In addition, in recent works the nonlinear energy-pumping phenomenon was studied in systems of coupled nonlinear oscillators. By energy pumping we denote the passive targeted energy transfer of vibration energy transfers from a primary (linear) system where it is originally generated (a chain of linear oscillators in this work) to a pre-assigned essentially nonlinear local attachment, termed nonlinear energy sink—NES (a strongly nonlinear end attachment in this work), where the vibration energy is localized and dissipated without 'spreading back' to the primary system [30–32]. In recent applications the concept of passively transferring and dissipating energy from a primary structure to strongly nonlinear attachments has been successfully applied to diverse engineering applications, including:

- shock isolation of impulsively loaded discrete and continuous vibrating systems [34];
- passive aeroelastic instability (flutter) suppression [35];
- seismic mitigation [36];
- drill—string instability suppression in oil industry applications [37].

In this work, we aim to apply K–L decomposition to study nonlinear energy pumping in a chain of coupled linear oscillators (the primary system) with a strongly nonlinear (nonlinearizable) end attachment. In fact, one of the aims of this work is through K–L decomposition to show that a lightweight, essentially nonlinear end attachment (possessing as low as 0.5% of the total mass of the chain) can affect the global dynamics of the system to which it is attached. In particular, by analyzing the dynamics of energy pumping through K–L decomposition, one is able to identify the dimensionality of the governing (underlying) nonlinear dynamical mechanism, and create reliable low-order models that be utilized for further design tasks (such as, monitoring and diagnosis of developing faults and control of the system).

2. Energy pumping phenomena in the linear chain with nonlinear end attachment

We consider the system depicted in Fig. 1, composed of a chain of 10 strongly coupled linear oscillators (designated as the 'primary system') with a strongly nonlinear (nonlinearizable) end attachment (designated as the 'NES'). The system possesses weak viscous damping, and the mass of the NES is assumed to be small compared to the overall mass of the chain. The governing equations of motion of the system are given by

$$\begin{aligned}
&\varepsilon\ddot{v} + \varepsilon\lambda(\dot{v} - \dot{y}_0) + C(v - y_0)^3 = 0,\\
&\ddot{y}_0 + \varepsilon\lambda\dot{y}_0 + \omega_0^2 y_0 - \varepsilon\lambda(\dot{v} - \dot{y}_0) - C(v - y_0)^3 + d(y_0 - y_1) = 0,\\
&\ddot{y}_j + \varepsilon\lambda\dot{y}_j + \omega_0^2 y_j + d(2y_j - y_{j-1} - y_{j+1}) = 0, \quad j = 1, \ldots, 8,\\
&\ddot{y}_9 + \varepsilon\lambda\dot{y}_9 + \omega_0^2 y_9 + d(y_9 - y_8) = 0,
\end{aligned} \tag{1a}$$

where we introduce the small parameter ε, $0 < \varepsilon \ll 1$, and all other parameters are assumed to be quantities of $O(1)$. In addition, we assume that the system is initially at rest, and that an impulse of magnitude F is applied at $t = 0$ at the left boundary of the linear chain, corresponding to the following initial conditions

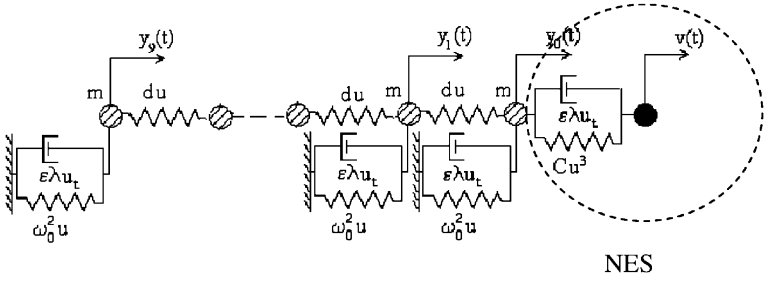

Fig. 1. The chain of linear coupled oscillations (the primary system) with strongly nonlinear end attachment (the NES).

for system (1a):

$$v(0) = \dot{v}(0) = 0, \quad y_p(0) = 0, \quad p = 0, \ldots, 9,$$
$$\dot{y}_k(0) = 0, \quad k = 0, \ldots, 8, \quad \dot{y}_9(0+) = F. \tag{1b}$$

In contrast to the classical linear vibration absorber, the proposed NES is capable of passively absorbing broadband energy from the linear chain. The underlying reason for this broadband energy absorption capacity is the essential (nonlinearizable) stiffness nonlinearity of the NES: since the NES possesses no preferential energy of oscillation (as its stiffness possesses no linear component), it can engage in resonance capture [38] with any mode of the chain (or sequentially with a set of chain modes in resonance capture cascades [32]) at arbitrary frequency ranges. The initial conditions dictate the precise scenario of resonance capture that is realized in each simulation, as well as the frequency content of the response of the NES. It follows that the NES is capable of multifrequency vibration energy pumping from the linear chain, a feature which is markedly distinct from the linear vibration absorber whose operation is narrowband. Moreover, the previous discussion leads to the conclusion that the lightweight, essentially nonlinear local attachment may induce global effects on the dynamics of the chain.

These claims are supported by the numerical results presented below. In Fig. 2 we present the transient responses $v(t)$ and $y_9(t)$ for a system with parameters $\varepsilon = 0.05$, $\lambda = 0.5$, $C = 0.1$, $\omega_0^2 = 1$, $d = 1$ and different

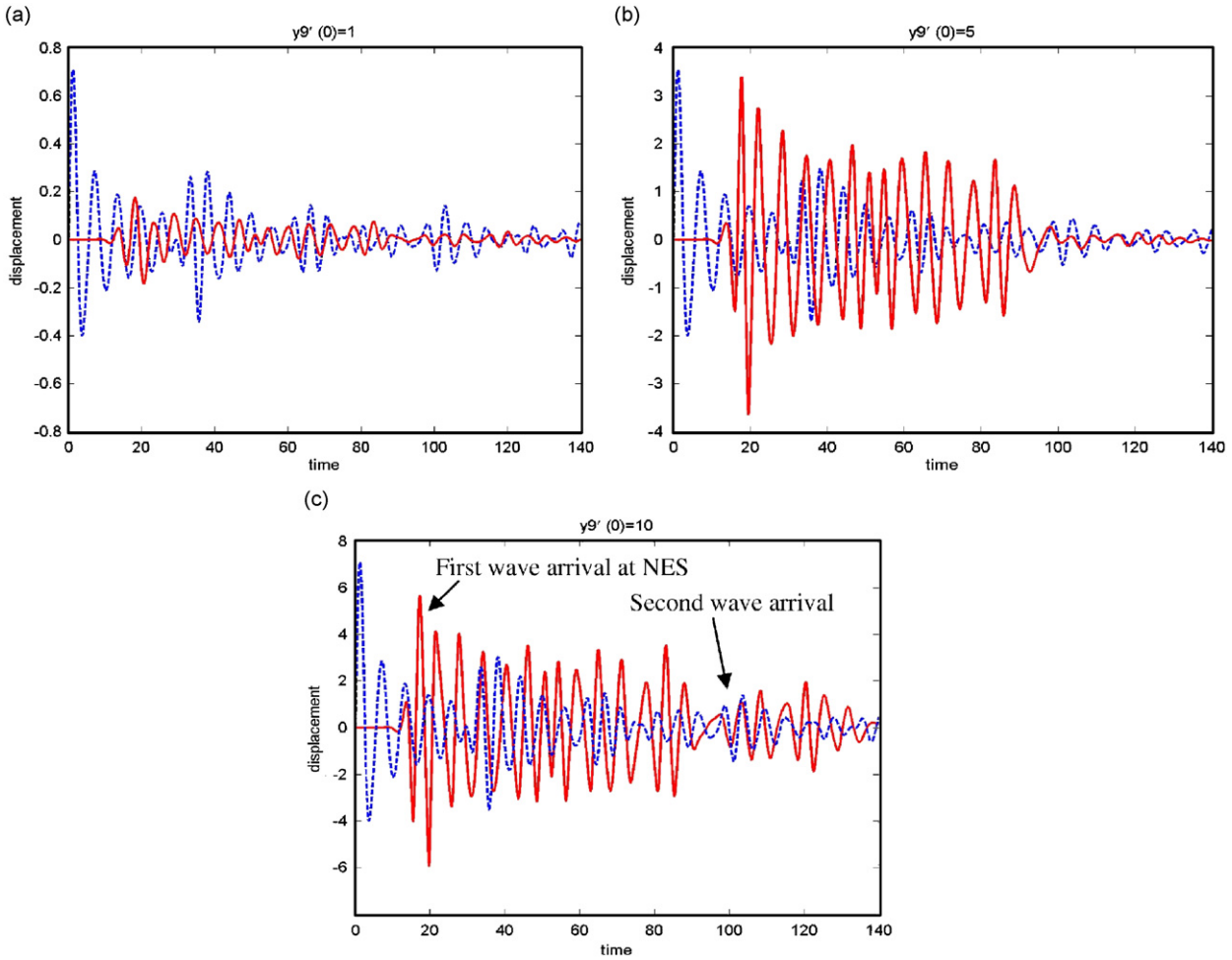

Fig. 2. Numerical transient responses of the nonlinear attachment and the directly forced particle of the chain ($v(t)$ ————, and $y_9(t)$ ----------) for impulses of different magnitudes, (a) $\dot{y}_9(0) = 1.0$, (b) $\dot{y}_9(0) = 5.0$, (c) $\dot{y}_9(0) = 10.0$.

magnitudes of applied impulse (unless otherwise noted, we will assume that these parameter values hold in the following simulations). We note that when the magnitude of the impulse is small [cf. Fig. 2(a)], no significant transfer of energy from the linear chain to the NES takes place; this is in agreement with the finding of previous works [30–32], that energy pumping is 'activated' above a critical energy threshold. With an increase of the magnitude of the impulse, the NES oscillates with significant amplitude [cf. Fig. 2(b) and (c)], indicating the occurrence of energy pumping from the chain to the NES. Examination of Fig. 2(c) corresponding to the highest energy level reveals two arrivals of wavepackets at the NES (the later corresponding to reflection of the main pulse from the left boundary of the chain); the NES is capable of absorbing and dissipating energy from both wavepackets.

To demonstrate the qualitatively different dynamics of the NES for weak and strong applied impulses, and the broadband energy pumping that occurs in the later case, in Fig. 3 we depict the numerical wavelet spectra of the relative response $v(t)-y_0(t)$ for impulses $\dot{y}_9(0) = 0.5$ and $\dot{y}_9(0) = 4.0$. We note at this point that the time derivative of the relative response $v(t)-y_0(t)$ denotes the relative deformation of the damper of the NES, and is directly related to the dissipation of vibration energy at the NES. The Matlab-based wavelet transform (WT) employed is this work was based on the algorithm developed at the Université de Liège by Dr. V. Lenaerts in collaboration with Dr. P. Argoul from the 'Ecole Nationale des Ponts et Chaussees'. Although the algorithm provides the opportunity to use two kinds of mother wavelets, namely Morlet and Cauchy, in the applications presented herein only the Morlet mother wavelet has been used. The WT can be regarded as a 'dynamic' extension of the 'static' Fourier Transform, in the sense that instead of decomposing a time series (signal) in the frequency domain using the cosine and sine trigonometric functions, alternative families of orthogonal functions are employed which are localized in frequency and time. These families of orthogonal functions, the so-called wavelets can be adapted in time and frequency so to provide details of the frequency components of the signal during the time interval that is analyzed. The wavelet spectra shown below depict the amplitude of the WT of the signal as function of frequency (vertical axis) and time (horizontal axis). Heavy shaded areas

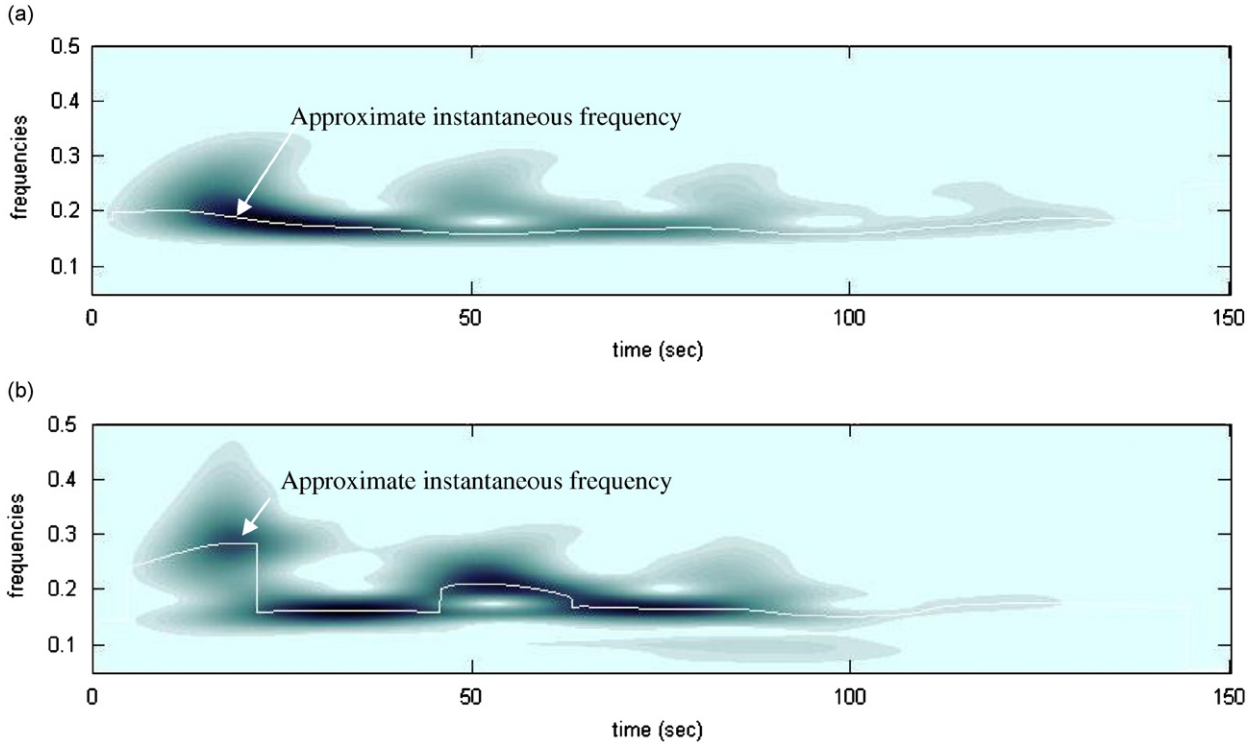

Fig. 3. Wavelet transform spectra of the relative response $v(t)-y_0(t)$ for weak and strong applied impulses: (a) $\dot{y}_9(0) = 0.5$, (b) $\dot{y}_9(0) = 4.0$ (frequencies in Hz).

correspond to regions where the amplitudes of the wavelet spectrum are high, whereas lightly shaded ones correspond to low amplitudes of the WT. Such plots enable one to deduce the temporal evolutions of the dominant frequency components of the signals analyzed, as well as, transitions between different modes that participate in the transient nonlinear responses [39,40].

Referring to Fig. 3a, when the weak impulse is applied, the NES seems to engage in resonance capture only with the lowest (in-phase) mode of the chain (at frequency 0.159 Hz); this is inferred by studying the approximate instantaneous frequency of the relative displacement (which is depicted by the continuous line connecting the maxima of the wavelet spectrum of Fig. 3a). On the contrary, for strong applied impulse the NES seems to engage in resonance capture with a series of modes of the chain, as inferred by the wavelet spectrum of Fig. 3b; initially, the dynamics of the NES engages in resonance capture with the highest (anti-phase) chain mode at 0.276 Hz; following an 'escape' from this relatively high-frequency resonance capture the dynamics of the NES engages in resonance with the low in-phase chain mode, before 'escaping' again and engaging in resonance capture with a high-frequency chain mode, and then finally setting into final resonance capture again with the in-phase mode. As a result, for the case of stronger applied impulse the response of the NES possesses multifrequency content and acts as a more efficient energy absorber (and dissipater) compared to the weak-impulse case.

To quantify the strength of energy pumping in the system we introduce at this point the following normalized energy dissipated by the NES:

$$H(t)=\frac{\varepsilon\lambda\int_0^t[\dot{v}(\tau)-\dot{y}_0(\tau)]^2\,\mathrm{d}\tau}{E_{\mathrm{input}}}\times 100,\quad E_{\mathrm{input}}=\frac{1}{2}\dot{y}_9(0)^2. \tag{2a}$$

This represents the percentage of input energy that is dissipated by the NES at time t. Since the system considered is passive the measure $H(t)$ reaches an asymptotic limit, which is designated as the energy measure of dissipation (EMD) H:

$$H=\lim_{t\to\infty}H(t)\approx\frac{\varepsilon\lambda\int_0^{T_d}[\dot{v}(\tau)-\dot{y}_0(\tau)]^2\,\mathrm{d}\tau}{E_{\mathrm{input}}}\times 100. \tag{2b}$$

The EMD is the energy that is eventually dissipated by the NES; in the computation we select the time window of the integration, T_d, to be sufficiently large in order to approximate as accurately as possible the asymptotic value (2b).

In Fig. 4a we present the plot of EDM as function of the stiffness characteristic C of the NES, for impulse strength $\dot{y}_9(0)=4.3$, for system parameters $\omega_0^2=1.0$, $d=2.0$, and two values of damping, namely, $\varepsilon\lambda=0.0125$, 0.025. For comparison, we also depict the corresponding EDMs for a chain with linear (instead of strongly nonlinear) attachment and identical parameter values. Clearly, the linear attachment proves to be effective only in a narrow band of small stiffness values, e.g., at stiffness where the (constant) resonance frequency of the linear attachment matches the frequency of a mode of the chain. On the contrary, the NES proves to be more effective than the linear absorber, since it proves to be capable of absorbing a significant part of the energy of the chain over a wider range of values of C, a feature which is due to its capacity to engage in resonance capture and passively absorb energy from *any* of the modes of the chain. We note that as much as 37% of input energy is passively absorbed and eventually dissipated by the NES, and that, even away from the region of optimal energy pumping, the NES maintains a steady value of significant energy pumping. In Fig. 4b we depict the 'optimal' normalized dissipated energy time histories $H(t)$ (expression (2a) for $\varepsilon\lambda=0.0125$ and for both cases of linear and nonlinear attachments. It is interesting to note that the consequent arrivals of wavepackets at the attachment are associated with sudden increases of the rates of energy dissipation, which can be clearly inferred in the plot.

The previous results indicate that the local addition of (even) a lightweight (in the examples considered the NES mass amounts to 0.5% of the total mass of the chain), strongly nonlinear NES can influence the global dynamics of the chain. In the following sections we will study in detail this global change of the dynamics by employing K–L decomposition, in an effort to study the dimensionality of the energy pumping phenomenon, to understand the governing dynamical mechanism that is responsible for energy pumping, and to create

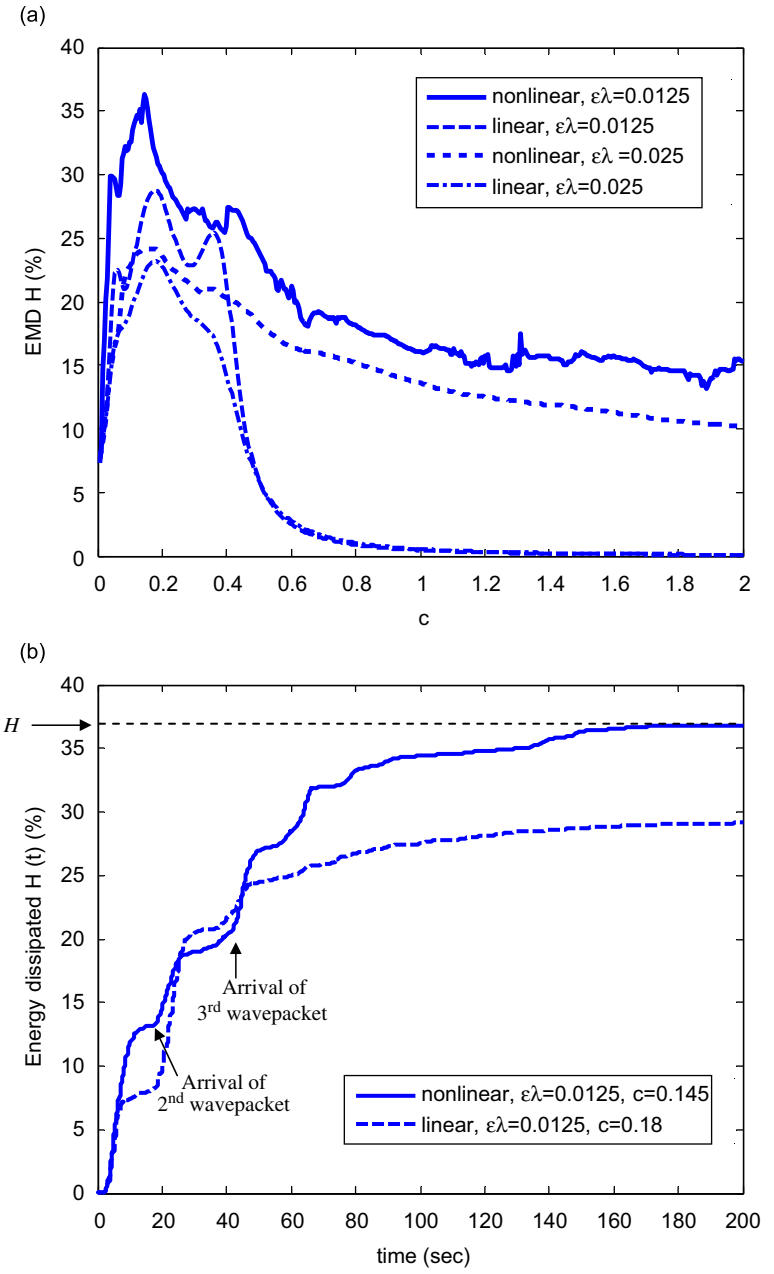

Fig. 4. Portion of input energy dissipated by the attachment for impulse magnitude $\dot{y}_9(0) = 4.3$, and $d = 2.0$: (a) EMD H for varying stiffness parameter C, comparison between strongly nonlinear and linear attachments for two values of damping; (b) time histories of energy dissipation for specific values of C and $\varepsilon\lambda = 0.0125$.

reliable low-order models of the dynamics. Moreover, in contrast to the linear absorber whose action is confined to a narrow range of the parameter C, the NES is capable of absorbing significant amounts of the input energy over wide ranges of this parameter; this is due to the fact that, since the NES is lacking a preferential resonance frequency (as it is an essentially nonlinear element), it can engage in resonance capture and passively absorb energy from any mode of the linear chain (note that none of the chain modes possesses a node at the point of attachment with the NES).

3. K–L modes of the combined chain—NES system

The K–L decomposition is now employed to study the dynamics of systems (1a) and (1b). Considering a scalar field $v(\underline{x}, t)$, $\underline{x} \in R^N$ defined in some spatiotemporal domain, at a given time instant t_i the system displays a snapshot $v_i \equiv v(\underline{x}, t = t_i)$. K–L decomposition seeks the most typical set of orthogonal functions (termed the K–L modes) $\{\phi\}$ that approximates the ensemble of snapshots in a least square sense. The solution of the minimization of the residue sum of squares between the actual snapshots and their approximation using the K–L modes leads to the following eigenvalue problem:

$$\mathbf{K}\phi = \hat{\lambda}\phi, \tag{3}$$

where $\mathbf{K} = \Sigma v_i v_i^{\mathrm{T}}$ and ϕ is a K–L mode shape. The corresponding eigenvalue, $\hat{\lambda}$, are the indicators of energy captured by the corresponding K–L modes, with the dominant K–L modes corresponding to the highest eigenvalues.

In the application considered in this work, the scalar field v includes the displacement of the 11 particles of the chain-NES system. The so-called 'direct method' is used to compute the K–L modes [16–20]. In Fig. 5a we depict the mode shapes of the four dominant K–L modes of the system for three different excitation cases as shown in Fig. 2 (small to high) and $C = 0.1$; for the K–L computation we used the simulated time series in the window $0 < t < 140$, since after that time the response of the system was negligible. For comparison purposes we also depicted the mode shapes of the four dominant K–L modes of the linear chain with no NES attached, under identical forcing conditions (in the linear case the results of K–L decomposition do not depend on the magnitude of the impulse, so only one set of 'linear' K–L modes is displayed). In the following discussion we will be referring to the K–L modes of the chain with and without NES as, 'nonlinear K–L modes' and 'linear K–L modes', respectively.

In Fig. 5b we display the variation of the percentage of energy (e.g., the normalized K–L eigenvalue) captured by each of the dominant four K–L modes for $C = 0.1$ and varying impulse magnitudes $\dot{y}_9(0)$. Superimposed to the plot of Fig. 5b is the EMD H, indicating the efficiency of vibration energy pumping by the NES.

Referring to the K–L decomposition of Fig. 5, we make the following observations:

(a) For weak applied impulse ($\dot{y}_9(0) = 1.0$) the nonlinear K–L mode shapes are nearly identical to the linear ones (cf. Fig. 5a), and the dominant four nonlinear K–L modes capture 78.18% of the total energy of the time series. In this case the amplitude of vibration is small, so that the nonlinear effects are also small, and the NES is not capable of significantly affecting the dynamics of the chain; moreover, the amplitude of the NES in the dominant nonlinear K–L modes is negligible (e.g., $v \approx -0.0733$ in the first K–L mode), and the corresponding EMD H is also small (cf. Fig. 5b). Finally, we note that for weak impulses the nonlinear K–L mode shapes are spatially extended (e.g., there is no spatial localization of the mode shapes).

(b) For strong applied impulses ($\dot{y}_9(0) = 5.0,\ 10.0$) the K–L decomposition results are drastically different. Indeed, the mode shapes of the nonlinear K–L modes are markedly different from the corresponding linear ones, which demonstrates that at higher energy levels the (local lightweight) NES affects drastically the global dynamics of the chain dynamics; the most important effect is the higher amplitude of the NES in the dominant nonlinear K–L modes, especially in the (most important) first K–L mode. In fact, for stronger impulses the first nonlinear K–L mode shape becomes localized in the neighborhood of the NES (with $v \approx -0.744$ for $\dot{y}_9(0) = 5.0$), whereas the other dominant nonlinear K–L modes remain spatially extended, with the NES, however, exhibiting finite motions. The localization of the first nonlinear K–L mode shape at the NES for stronger impulses is an indication of transfer of energy from the chain towards the NES, and, hence, of passive energy pumping.

(c) Considering the percentages of energy in the four dominant nonlinear K–L modes (cf. Fig. 5b), we note that until the critical threshold $\dot{y}_9(0) = 1.6$, the total percentage of energy captured by these modes is small, indicating multidimensionality of the dynamics. Above that critical threshold, however, there occurs a rapid increase of the percentage of energy captured by the first nonlinear K–L mode, indicating that this mode becomes increasingly more dominant in the response; at the same time (as discussed previously) the spatial shape of this mode becomes strongly localized at the NES, indicating energy pumping from the

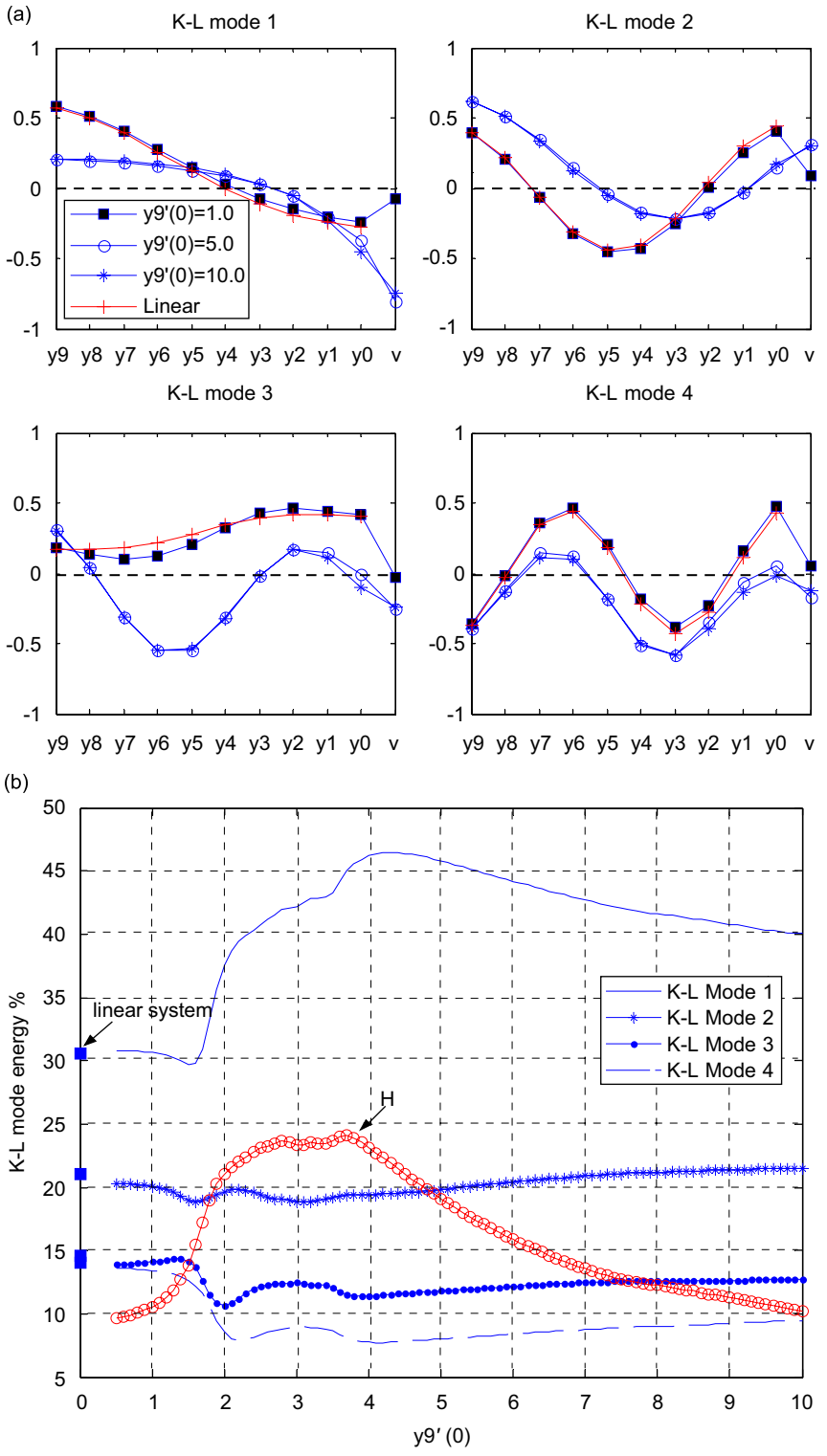

Fig. 5. K–L decomposition of the chain-NES system: (a) mode shapes of the four dominant K–L modes for $C = 0.1$ and $\dot{y}_9(0) = 1.0,\ 5.0$ and 10.0 (the K–L modes of the linear chain without NES are also depicted); (b) percentage of energy captured by each of the four dominant K–L modes for varying impulse magnitudes $\dot{y}_9(0)$ and corresponding energy dissipation measure H (-o-o-o-o-).

linear primary system (chain) to the NES. This is confirmed by the significant increase of the EMD H as the critical threshold $\dot{y}_9(0) = 1.6$ is exceeded, which shows that the increased dominance of the first, localized K–L mode in the response is primarily responsible for enhanced energy pumping in the system.

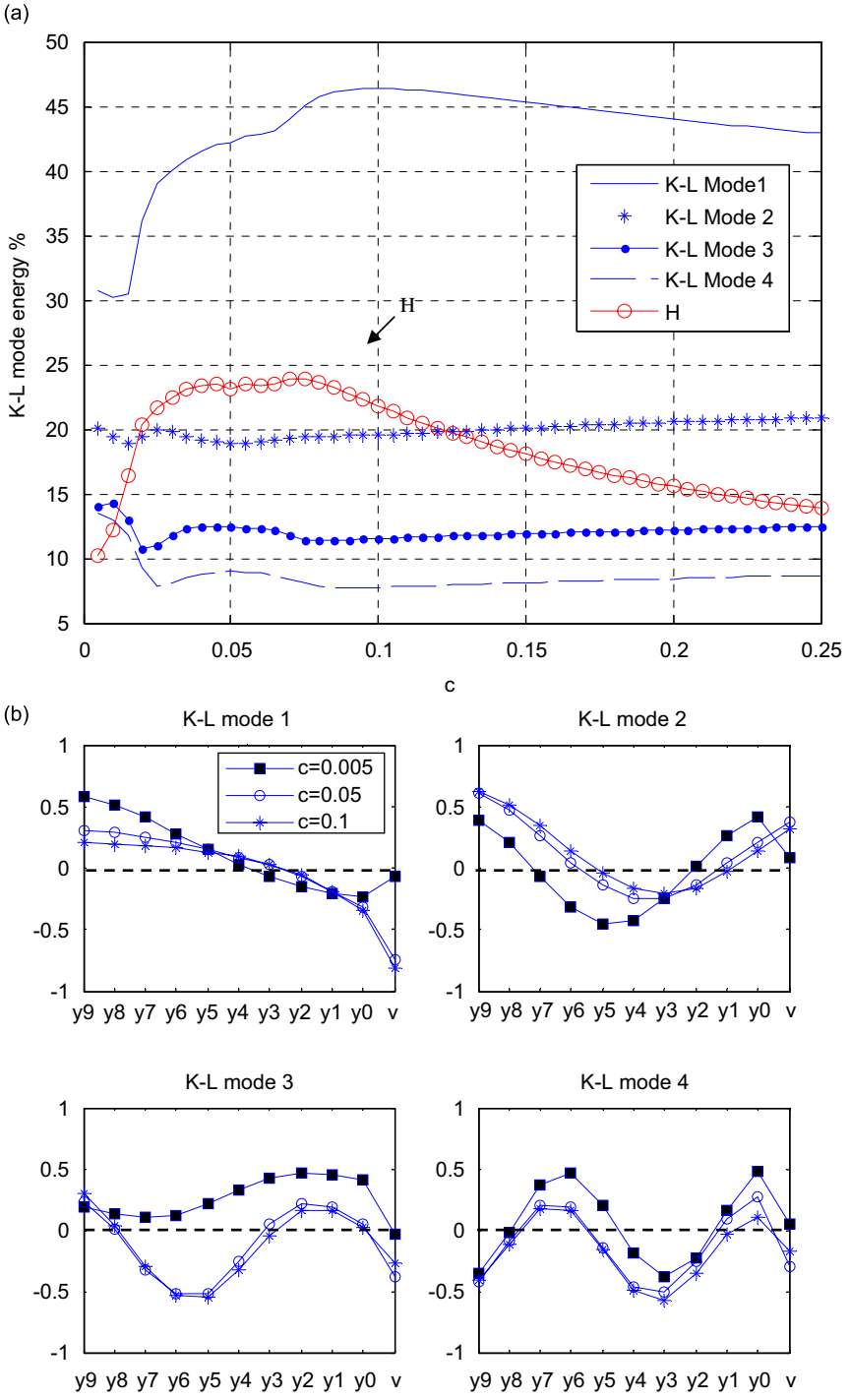

Fig. 6. K–L decomposition of the chain-NES system: (a) percentage of energy captured by each of the four dominant K–L modes for $\dot{y}_9(0) = 4.3$ and varying nonlinear stiffness characteristic C; the corresponding energy dissipation measure H (-o-o-o-o-o-) is also depicted; (b) mode shapes of the four dominant K–L modes for $\dot{y}_9(0) = 4.3$ and $C = 0.005$, 0.05 and 0.1.

This conclusion is also confirmed by the observation that when this trend reverses and H decreases for impulse magnitudes above $\dot{y}_9(0) = 4.3$, the percentage of energy captured by the first (still localized at the NES) mode also decreases, and the energy percentages of the other (non-localized) K–L modes gradually increase.

(d) An additional conclusion is that in the regime of increased energy pumping (e.g., $1.6 < \dot{y}_9(0) < 4.3$), the dimensionality of the dynamics of the system decreases, as the first localized K–L mode captures a higher percentage of energy of the time series and the contribution of the remaining (non-localized) K–L modes diminishes. In fact, for $\dot{y}_9(0) = 5.0$ the four dominant K–L modes capture 85.42% of the total energy, and the first K–L mode nearly 46%, whereas, for $\dot{y}_9(0) = 10.0$ the dominant four K–L modes capture 83.68% of the energy, and the first K–L mode 40%. This implies that in regimes of strong energy pumping the transient dynamics of the system may be approximated by low-dimensional reduced-order models, a topic which is discussed in the next section.

Similar conclusions are drawn from the K–L decomposition results depicted in Fig. 6, for a chain-NES system forced by an impulse of magnitude $\dot{y}_9(0) = 4.3$ and varying nonlinear stiffness characteristic C. Again, enhanced energy pumping in this case is associated with an increase of the percentage of energy captured by the localized first dominant K–L mode of the dynamics, and a consequent decrease of the dimensionality of the dynamics.

In order to enhance energy pumping from the chain to the nonlinear end attachment, we now consider an alternative two-degree-of-freedom NES (2dof NES) configuration, composed of two particles and two strongly nonlinear stiffness in parallel to viscous dampers; the new NES configuration is presented in Fig. 7. We wish to compare the performance of the 2dof NES to that of the single-dof NES (sdof NES) considered up to this point. Similarly to the previous simulations the system is assumed to be initially at rest with an impulse applied at the left boundary of the chain at $t = 0$. Due to the alternative NES configuration used in this case, the EMD H is defined as

$$H = \frac{\varepsilon\lambda \int_0^{T_d} \{[\dot{v}_1(\tau) - \dot{y}_0(\tau)]^2 + [\dot{v}_2(\tau) - \dot{v}_1(\tau)]^2\}\, d\tau}{E_{\text{input}}} \times 100, \quad E_{\text{input}} = \frac{1}{2}\dot{y}_9(0)^2. \tag{4}$$

As in the previous NES, EMD represents the percentage of input energy that is eventually dissipated by the two viscous dampers of the 2dof NES.

In Fig. 8 we perform K–L decomposition of the dynamics of the chain with a 2dof NES, impulse magnitude equal to $\dot{y}_9(0) = 4.3$, $C_1 = 0.5$ and varying C_2. The chain parameters for these simulations were selected as, $\omega_0^2 = 1.0$, $d = 2.0$, the damping as, $\varepsilon\lambda = 0.025$, and the mass of each of the two masses of the NES as, $\varepsilon = 0.05$. Hence, in this series of simulations the 2dof NES possesses double the mass of the previously considered sdof NES, and equals 1% the entire mass of the chain. In this case we notice that as much as 40% of the input energy can be passively absorbed and dissipated by the 2dof NES. In Fig. 9 we study the efficiency of energy pumping of the 2dof NES as function of input energy, for $C_1 = 0.5$, $C_2 = 0.055$. We note that the 2dof NES dissipates more than 30% of the input energy in the chain for impulses in the range $\dot{y}_9(0) = 2.2 \sim 10$. It follows that 2dof NES provides more efficient and robust energy pumping compared to the sdof NES. In addition, there are similar trends regarding the coherence of K–L mode shapes, the strong dominance of the first K–L mode over the others in the regime of strong energy pumping, and the localization of the first K–L mode shape

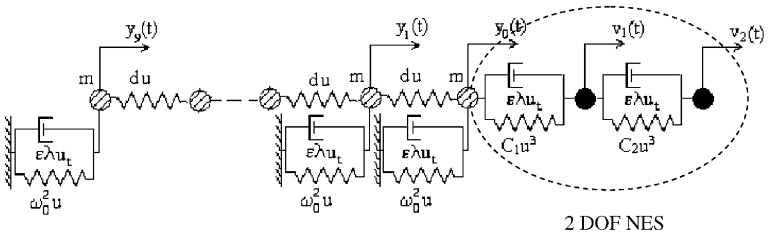

Fig. 7. The chain of linear coupled oscillations (the primary system) with strongly nonlinear two degree-of-freedom end attachment (the NES).

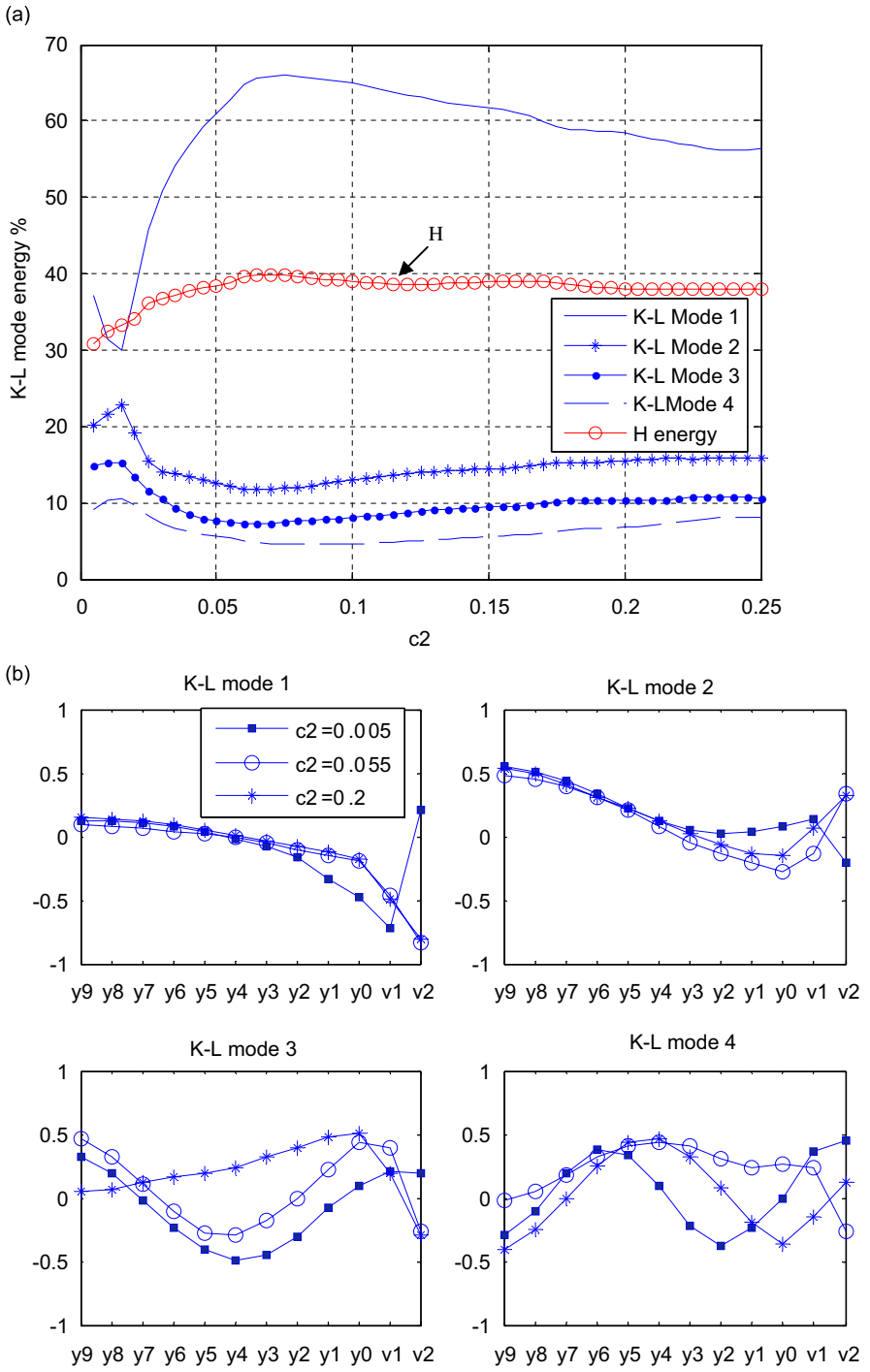

Fig. 8. Chain with 2dof NES, percentages of energy captured by the four dominant K–L modes, superimposed to the EDM H: (a) $\dot{y}_9(0) = 4.3$, $C_1 = 0.5$ and varying C_2; (b) K–L mode shapes for $\dot{y}_9(0) = 4.3$, $C_1 = 0.5$ and $C_2 = 0.005$, 0.05, 0.2.

in the 2dof NES when C_2 increases. Similar trends are observed in the K–L results of Fig. 9, for a system with $C_1 = 0.5$, $C_2 = 0.055$ and varying impulse magnitude $\dot{y}_9(0)$.

A general conclusion from the K–L decomposition analysis carried out in this section is that the first localized K–L mode is dominant in the strong energy pumping regime and appears to govern the dynamics of

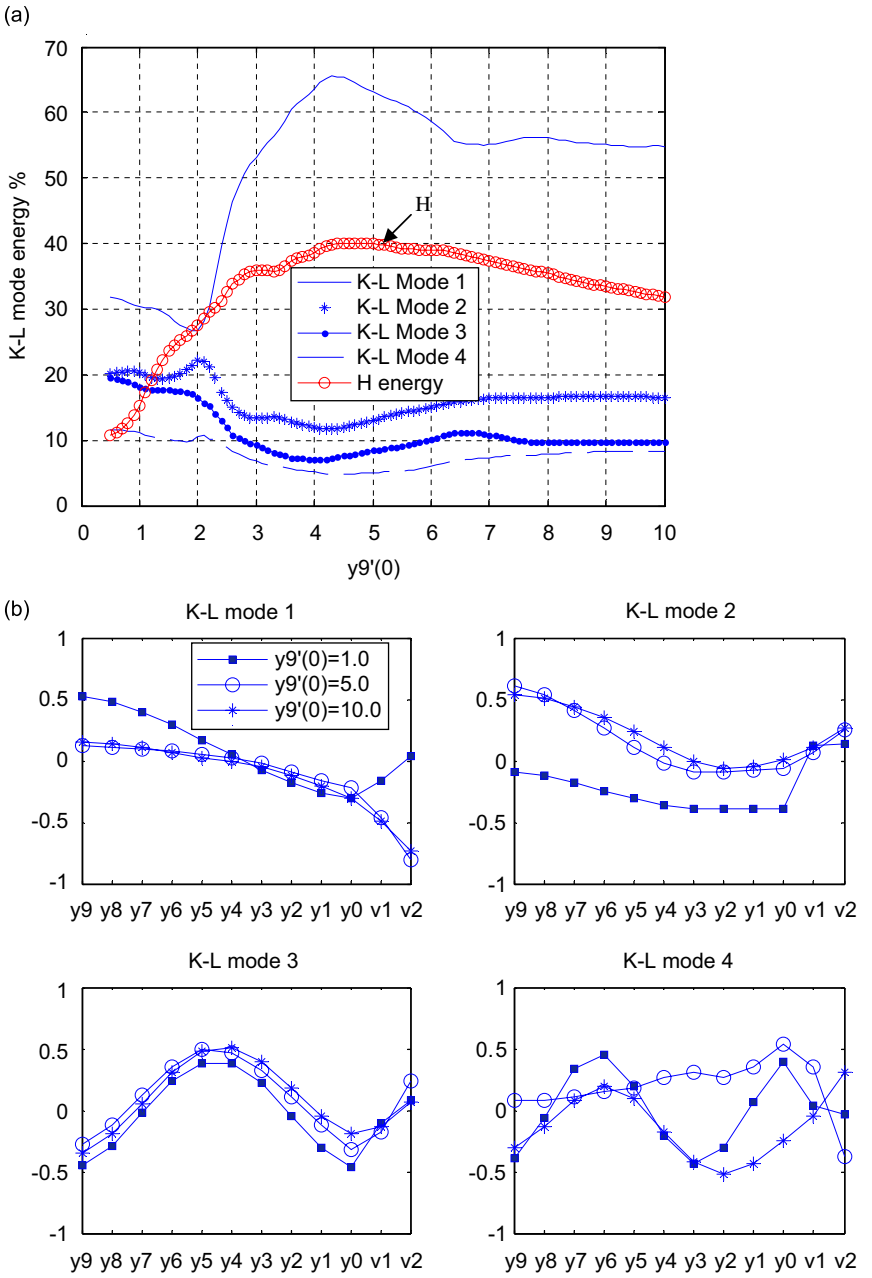

Fig. 9. Chain with 2dof NES, percentages of energy captured by the four dominant K–L modes, superimposed to the EDM H: (a) $C_1 = 0.5$, $C_2 = 0.055$ and varying impulse magnitudes $\dot{y}_9(0)$; (b) K–L mode shapes for $C_1 = 0.5$, $C_2 = 0.055$ and $\dot{y}_9(0) = 1.0,\ 5.0,\ 10.0$.

passive energy transfer; moreover, the increase of energy captured by the first K–L mode when strong energy pumping occurs indicates that the dimensionality of the corresponding dynamics decreases, so that accurate reduced-order models can be constructed by taking into account only a few leading K–L modes (by construction these modes possess an orthogonal structure). Another interesting observation regarding the system with a sdof NES is that the four leading (dominant) K–L modes are similar, both in terms of mode shape and in terms of energy distribution for the two cases of enhanced energy pumping, e.g., when $\dot{y}_9(0) = 5.0$ and $\dot{y}_9(0) = 10.0$. This suggests that the mode shape derived from one excitation condition can be used as a low-dimensional model for another excitation case under the condition that their K–L modes are similar. This

finding paves the way for using a single low-dimensional model over a range of different initial and forcing conditions. In the following section, we study the construction of low-dimensional reduced-order models for the case of the sdof NES.

4. Reduced-order modeling and multiple correlation coefficient

The nonlinear system governed by the system (1a) and (1b) can be expressed by the equation

$$\mathbf{M}\ddot{\mathbf{Y}}(t) + \mathbf{C}\mathbf{Y}(t) + \mathbf{K}\mathbf{Y}(t) + \mathbf{N}(\mathbf{Y}(t), \dot{\mathbf{Y}}(t)) = 0, \tag{5}$$

where $\mathbf{M}$, $\mathbf{C}$ and $\mathbf{K}$ are the mass, damping and stiffness matrices, $\mathbf{Y}(t) = [v, y_0, y_1, \ldots, y_9]^{\mathrm{T}}$ the vector of displacements, and $\mathbf{N}(\mathbf{Y}(t), \dot{\mathbf{Y}}(t))$ the nonlinear term. Performing K–L decomposition, a (11×4) matrix $\mathbf{U}$ is generated composed of the four leading K–L modes. Ideally, to construct accurate reduced-order models one would need to include in the analysis the K–L modes that capture a total of 99% of the energy of the simulated time series (e.g., K–L modes with corresponding sum of eigenvalues equal to 99% of the sum of all eigenvalues). In this section we focus on the system depicted in Fig. 1 with parameters $\varepsilon = 0.05$, $\lambda = 0.5$, $C = 0.1$, $\omega_0^2 = 1$, $d = 1$; in this case it can be shown that 7–8 K–L modes capture 99% of the energy of the time series. Instead, in the following analysis we used only the leading 4 K–L modes in the order reduction process, since this number was deemed sufficient for the accurate reconstruction of the signals; at the end, one expects relatively small errors in the reduced-order signal reconstructions.

Assuming that all the vectors have zero mean value, the system response $\mathbf{Y}(t)$ is expressed as

$$\mathbf{Y}(t) = \mathbf{U}\mathbf{X}(t). \tag{6}$$

Substituting Eq. (6) into Eq. (5), pre-multiplying by $(\mathbf{MU})^{-1}$, and taking into account the orthogonality properties of the matrix of K–L modes $\mathbf{U}$, one obtains the following lower order model:

$$\ddot{\mathbf{X}}(t) + \mathbf{C}_{\mathrm{new}}\dot{\mathbf{X}}(t) + \mathbf{K}_{\mathrm{new}}\mathbf{X}(t) + (\mathbf{MU})^{-1}\mathbf{N}(\mathbf{X}(t), \dot{\mathbf{X}}(t)) = 0, \tag{7}$$

where $\mathbf{C}_{\mathrm{new}} = (\mathbf{MU})^{-1}\mathbf{CU}$, and $\mathbf{K}_{\mathrm{new}} = (\mathbf{MU})^{-1}\mathbf{KU}$. Eq. (7) can be solved and then used to reconstruct the system response through (6). When a different matrix $\mathbf{U}$ consisting of K–L modes corresponding to a certain initial condition is substituted into Eq. (7), the low-order model corresponding to this initial condition is constructed.

The low-dimensional model based on the K–L modes derived from analysis of the time series corresponding to the initial condition $\dot{y}_9(0) = 1.0$ (when no significant energy pumping occurs as shown in Fig. 2a) is written below:

$$\ddot{\mathbf{X}}(t) + \begin{bmatrix} 0.0268 & -0.0030 & -0.0023 & -0.0031 \\ -0.0032 & 0.0301 & 0.0039 & 0.0054 \\ -0.0032 & 0.0052 & 0.0290 & 0.0055 \\ -0.0037 & 0.0059 & 0.0046 & 0.0313 \end{bmatrix}$$

$$\dot{\mathbf{X}}(t) + \begin{bmatrix} 1.0842 & 0.0299 & -0.0326 & -0.0203 \\ 0.0318 & 1.3794 & 0.0232 & -0.0176 \\ -0.0328 & 0.0225 & 1.0386 & -0.1288 \\ -0.0170 & -0.0202 & -0.1274 & 1.8031 \end{bmatrix}$$

$$\mathbf{X}(t) + \begin{bmatrix} -0.0037 & -0.2409 \\ 0.0045 & 0.4140 \\ -0.0017 & 0.4155 \\ 0.0027 & 0.4782 \end{bmatrix} \begin{bmatrix} C(\Delta)^3 \\ -C(\Delta)^3 \end{bmatrix} = 0 \tag{8}$$

$$\Delta = v - y_0 = [-0.0733 \quad 0.0879 \quad -0.0335 \quad 0.0538]\mathbf{X}(t) - [-0.2361 \quad 0.4082 \quad 0.4177 \quad 0.4747]\mathbf{X}(t).$$

The initial condition $\dot{y}_9(0) = 1.0$ is transformed to $\dot{\mathbf{X}}(0) = [0.5784 \quad 0.3919 \quad 0.1815 \quad -0.3590]^{\mathrm{T}}$ in the low-order model. The reconstruction of the time series for $y_1(t)$ using the above model is shown in Fig. 10a. We can see that the reconstruction of the system response compares well with the direct numerical simulation, which suggests that the four K–L-based low reduced-order model is sufficient to accurately reconstruct the system response. It follows that the 4dof, K–L-based reduced-order model is capable of modeling the dynamics of the original 11dof system.

Similarly we can construct a K–L-based reduced-order model for the energy-pumping regime. Expression (9) represents the reduced-order model based on the four dominant K–L modes derived by analyzing the time series corresponding to the initial condition $\dot{y}_9(0) = 5.0$ (as shown in Fig. 2b):

$$\ddot{\mathbf{X}}(t) + \begin{bmatrix} 0.0867 & -0.0235 & 0.0145 & 0.00701 \\ -0.0236 & 0.0340 & -0.0055 & -0.0027 \\ 0.0160 & -0.0061 & 0.0288 & 0.0019 \\ 0.0090 & -0.0034 & 0.0022 & 0.0261 \end{bmatrix} \dot{\mathbf{X}}(t) + \begin{bmatrix} 1.3114 & -0.2560 & 0.2567 & -0.3550 \\ -0.1266 & 1.2681 & -0.0264 & 0.2153 \\ 0.0796 & 0.0012 & 1.5308 & -0.3307 \\ -0.0142 & 0.0573 & -0.1874 & 1.4463 \end{bmatrix} \mathbf{X}(t) + \begin{bmatrix} -0.2422 & -2.0108 \\ 0.0928 & 0.7682 \\ -0.0753 & -0.5182 \\ -0.0512 & -0.2874 \end{bmatrix} \begin{bmatrix} C(\Delta)^3 \\ -C(\Delta)^3 \end{bmatrix} = 0 \tag{9}$$

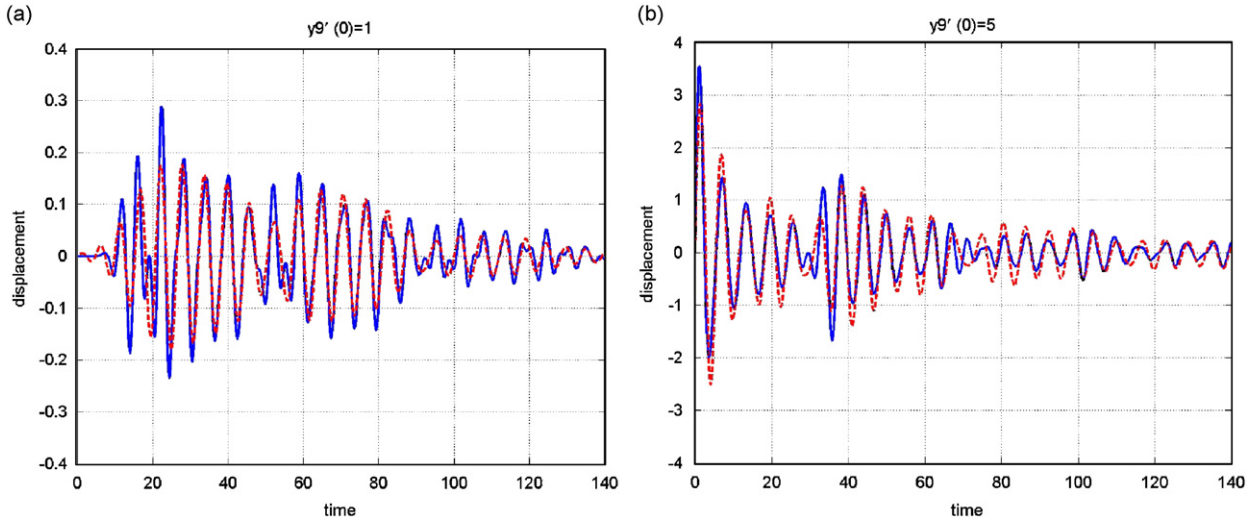

Fig. 10. Exact versus reconstructed responses: (a) $y_1(t)$ (———— simulation, ---------- reconstruction) using the 4dof reduced-order model (8); (b) $y_9(t)$ (———— simulation, ---------- reconstruction) using the 4dof reduced-order model (9).

$$\Delta = [-0.8055 \quad 0.3087 \quad -0.2504 \quad -0.1702]\mathbf{X}(t) - [-0.3754 \quad 0.1414 \quad -0.0098 \quad 0.0582]\mathbf{X}(t).$$

This model is used to reconstruct the time response of $y_9(t)$ as shown in Fig. 9b. The initial condition becomes $\dot{\mathbf{X}}(0) = [1.0519 \quad 3.0691 \quad 1.5448 \quad -1.9886]^{\mathrm{T}}$. Again, good agreement with direct numerical simulation is observed, validating the accuracy of the reduced-order model in this case as well.

In order to quantify the applicability of the K–L-based reduced-order models to different initial conditions (or excitations) than the ones for which they were originally derived, an indicator that can measure the similarity of the system response under different initial conditions is required. The absolute error between different responses can be used as such indicator, but it has the disadvantage that it lacks comparability; indeed, one cannot decide easily how much error constitutes the maximum absolute tolerance. In this work we propose the use of a MCC as the indicator for providing a normalized error estimation when comparing system responses subject to different initial conditions. The MCC is traditionally applied to study data regression and is closely related to residual variance and standard error of estimate in the regression.

In Ref. [33] the MCC was introduced to study $\hat{Y}$, the regression of a variable Y by multiple variables X_1, $X_2, \ldots X_k$, with each variable representing a data series. Assuming that all variables are normalized and have zero mean, the MCC is defined as

$$R^2_{Y\hat{Y}} = \left(\sum_{i=1}^{k} \mathbf{B}_i \cdot \sum X_i Y\right) \Big/ \sum Y^2, \tag{10}$$

where matrix $\mathbf{B}$ consists of the regression coefficients. The MCC gives an indication of how well the variable Y can be predicted by the multiple variables X_1, $X_2, \ldots, X_k$; $R^2_{Y\hat{Y}}$ is related to the residue sum of square error between the prediction and the actual data series, where

$$R^2_{Y\hat{Y}} = 1 - \frac{SS_{\mathrm{res}}}{SS_{\mathrm{tol}}} = 1 - \frac{\sum (Y - \hat{Y})^2}{\sum Y^2} \quad \text{and} \quad \hat{Y} = \mathbf{B}X.$$

In this work, the low-order model derived by analyzing the response corresponding to a specific initial condition (for example, $\dot{y}_9(0) = 5.0$) is based on the matrix $\mathbf{U}_5$ composed of its own first 4 K–L modes. Let us denote by $\mathbf{X}_5(t)$ the displacement vector computed by the low-order model derived for the initial condition $\dot{y}_9(0) = 5.0$, and $\mathbf{Y}_5(t)$ the displacement vector of the full-order model; then $\mathbf{U}_5$ provides the regression coefficients in $\mathbf{B}$. By substituting $\mathbf{X}_5(t)$, the displacement variables of $\mathbf{Y}_5(t)$ and $\mathbf{U}_5$ into Eq. (10) we can compute the MCCs of the variables in $\mathbf{Y}_5$ by $\mathbf{X}_5$. When we use this specific low-order model to approximate the response for other initial conditions (such as when $\dot{y}_9(0) = 10.0$), we still use the matrix $\mathbf{U}_5$ (based on the 4 K–L modes derived by the initial condition $\dot{y}_9(0) = 5.0$) to compute $\mathbf{X}_{10}$, rather than the matrix $\mathbf{U}_{10}$ derived from the other initial condition (in this case $\dot{y}_9(0) = 10.0$). Then, the vector $\mathbf{X}_{10}$ and matrix $\mathbf{U}_5$ are substituted into Eq. (10) to compute the MCCs of the response variables in $\mathbf{Y}_{10}$. This process is repeated for initial conditions $\dot{y}_9(0)$ in the range 0.5–10 to derive the result depicted in Fig. 11. Considering these results, one can see that the MCC of $v(t)$ changes drastically from 0.081 to 0.937 in the region where $\dot{y}_9(0)$ ranges from 0.5 to 2. This corresponds to the region of points of inflection in the curves of Fig. 5b. This suggests that the MCC curve is closely related to the different dynamical state of the system, and is a clear quantitative indicator of the transferability of the low-dimensional models of the system. From this figure we can see that to study systems with initial conditions $\dot{y}_9(0)$ ranging from 1.8 to 10.0, the low-dimensional model of Eq. (8), which corresponds to $\dot{y}_9(0) = 5.0$, can provide 90% of the accuracy that each specific low-dimensional model corresponding to different initial conditions can provide. Another important feature of the MCC is its computational efficiency. In real practices once a reduced-order model has been setup under a set of initial conditions, the matrix $\mathbf{B}$ has been decided, Vectors $\mathbf{X}$ and $\mathbf{Y}$ can then be measured as the output of the reduced-order model system and the full-order system. MCC for different initial conditions can be easily computed using Eq. (10). The operation count for computing MCC scales like $O(kN^2)$ if variable Y has N samples of data. This indicator can provide a fast and efficient way to measure the applicability of the reduced-order model under different conditions.

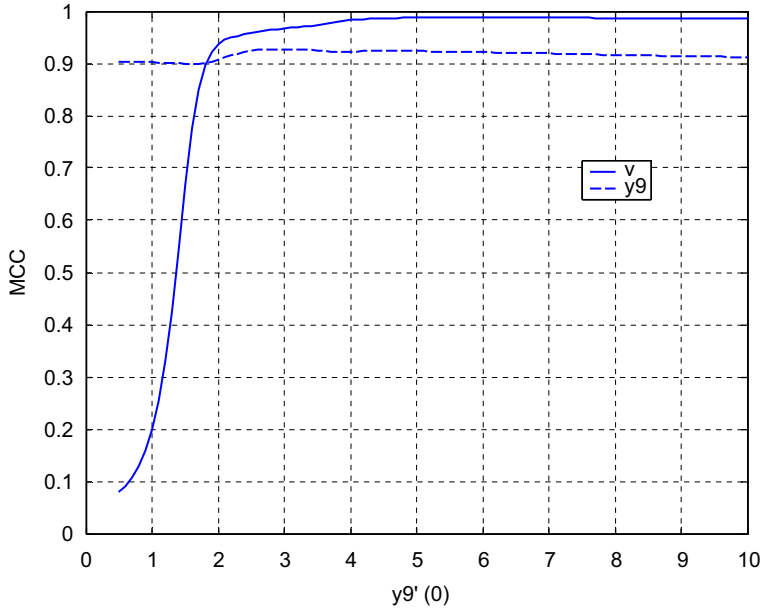

Fig. 11. The MCC of $v(t)$ and $y_9(t)$ for different impulse magnitudes $\dot{y}_9(0)$ based on the reduced-order model derived for $\dot{y}_9(0) = 5.0$.

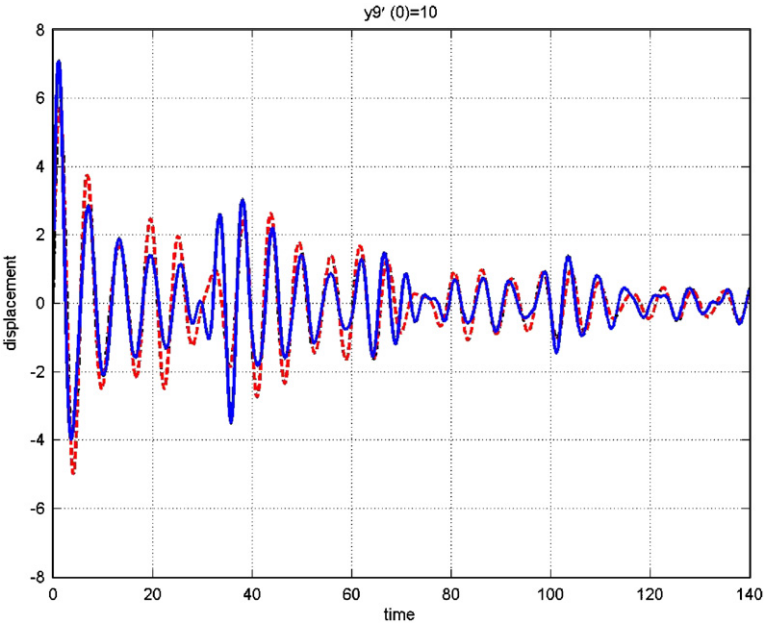

Fig. 12. Exact (————) versus reconstructed (----------) response of $y_7(t)$ for impulse magnitude $\dot{y}_9(0) = 10.0$; reconstruction was performed using the low-dimensional model derived from the case of impulse magnitude $\dot{y}_9(0) = 5.0$.

In Fig. 12 we provide a comparison between exact and reduced-order reconstructed responses. With dashed line we present the reconstruction of the response of $y_9(t)$ corresponding to initial impulse $\dot{y}_9(0) = 10.0$, using, however, the low-dimensional model of Eq. (8) created for an impulse of magnitude $\dot{y}_9(0) = 5.0$. In this case, the initial condition becomes $\dot{\mathbf{X}}(0) = [\,2.1037 \quad 6.1383 \quad 3.0895 \quad -3.9773\,]^{\mathrm{T}}$. We see that the reconstruction is comparable to the simulation. In this case the residue sum of squares error is 24.4% comparing with the error of 23.5% when we use its own low-dimensional model created for an impulse of magnitude $\dot{y}_9(0) = 10.0$. This shows the feasibility of the application of a low-dimensional model to a wider range of system conditions.

5. Concluding remarks

In this paper we present numerical evidence of energy pumping in a mechanical system consisting of a chain of linearly coupled oscillators with an essentially nonlinear, single-degree-of-freedom (sdof) end attachment. The chain was forced by an impulse applied to its free end, and the capacity of the nonlinear end attachment to passively absorb and locally dissipate a part of the impulsive energy was studied. We showed that, when the imparted energy exceeds a certain threshold, passive energy pumping from the chain to the NES occurs. The Karhunen–Loeve (K–L) decomposition method was applied to derive the dominant proper orthogonal modes of the system in the different regimes of the dynamics of the system. We showed that in the energy-pumping regime the dominant K–L mode localizes at the NES, and captures a high portion of the energy of the time series. In fact, we showed that in the energy pumping regime the leading K–L mode becomes increasingly more dominant over the other K–L modes, compared to the low-energy regime of the dynamics where no significant energy pumping occurs.

A study of the K–L mode shapes in the different regimes of the motion reveals that when the energy of the system is sufficiently high, the lightweight strongly nonlinear end attachment, although local and lightweight (it possesses 0.5% of the total mass of the chain), it can influence the global structure of the dynamics, e.g., the spatial distributions of all dominant K–L mode shapes. This due to the fact that the strongly nonlinear attachment possesses no linear stiffness term, and, hence, lacks a preferential resonance frequency; it follows that, depending on its instantaneous energy level, the strongly nonlinear attachment is capable of engaging in resonance capture with any mode of the chain, thus introducing non-local effects in the chain dynamics.

As shown in this work the efficiency and robustness of energy pumping can be enhanced by using a 2dof NES possessing two essential elements, though the main conclusions regarding the results of K–L decomposition in the energy pumping regime in this case are similar to the sdof NES.

In high dimensional or spatially extended dynamical systems, the construction of effective low-dimensional, reduced-order models is essential for design, monitoring and diagnosis of faults, and control purposes. We showed that K–L-based reduced-order models can be effective in reconstructing the dynamics of the high-dimensional systems considered herein, both before and in the energy-pumping regime. Moreover, we demonstrated the transferability of the reduced-order models for different initial conditions. We introduced a quantitative indicator, the MCC, which was shown to be effective in assessing the transferability of the derived K–L based low-dimensional models to varying initial conditions of the system; this knowledge is important when using such reduced-order models for control purposes or for other design applications.

References

[1] K. Karhunen, Under lineare methoden in der wahrscheinlichkeitsrechnung, *Annals of Academic Science Fennicae Series, A 1, Mathematical Physics* 37 (2) (1946).
[2] M.M. Loeve, *Probability Theory*, Von Nostrand, Princeton, NJ, 1955.
[3] L. Sirovich, M. Kirby, An eigenfunction approach to large scale transitional structures in jet flow, *Physics of Fluids* A2 (1989) 127–136.
[4] M. Rajaee, S.K.F. Karlsson, L. Sirovich, Low-dimensional description of free shear flow coherent structures and their dynamical behavior, *Journal of Fluid Mechanics* 258 (1994) 1–29.
[5] H. Tarman, A Karhunen–Loeve analysis of turbulent thermal convection, *International Journal for Numerical Methods in Fluids* 22 (1996) 67–79.
[6] A. Benguedouar, Proper Orthogonal Decomposition In Dynamical Modeling: A Qualitative Dynamic Approach, PhD Thesis, Boston University, Boston, MA, 1995.
[7] M.D. Graham, I.G. Kevrekedis, Alternative approaches to the Karhunen–Loeve decomposition for model reduction and data analysis, *Computers and Chemical Engineering* 20 (5) (1996) 495–506.
[8] D. Zheng, K.A. Hoo, System identification and model-based control for distributed parameter systems, *Computers and Chemical Engineering* 28 (8) (2004) 1361–1375.
[9] J.L. Lumley, The structure of inhomogeneous turbulent flows, in: A. M. Yaglom, V.I. Tatarski (Eds.), *Atmospheric Turbulence and Radio Wave Propagation*, Nauko, Moscow, 1967.
[10] J.L. Lumley, *Stochastic Tools in Turbulence*, Academic Press, New York, 1970.
[11] J.L. Lumley, *Transaction and Turbulence*, in: R.E. Meyer (Ed.), Academic Press, New York, 1981.
[12] L. Sirovich, Turbulence and the dynamics of coherent structures: part I—coherent structures, *Quarterly of Applied Mathematics* 45 (3) (1987) 561–571.

[13] J.P. Cusumano, M.T. Sharkady, B.W. Kimble, Dynamics of a flexible beam impact oscillator, *Philosophical Transactions of the Royal Society of London* 347 (1994) 421–438.
[14] I. Georgiou, I.B. Schwartz, Dynamics of large scale coupled structure/mechanical system: a singular perturbation/proper orthogonal decomposition approach, *SIAM Journal on Applied Mathematics* 59 (4) (1999) 1178–1207.
[15] I.T. Georgiou, I. Schwartz, E. Emaci, A. Vakakis, Interaction between slow and fast oscillations in an infinite degree-of-freedom linear system coupled to a nonlinear subsystem: theory and experiment, *Journal of Applied Mechanics* 66 (2) (1999) 448–459.
[16] M.F.A. Azeez, A.F. Vakakis, Proper orthogonal decomposition (POD) of a class of vibroimpact oscillations, *Journal of Sound and Vibration* 240 (5) (2001) 859–889.
[17] X. Ma, A.F. Vakakis, Karhunen–Loeve decomposition of the transient dynamics of a multibay truss, *AIAA Journal* 37 (8) (1999) 939–946.
[18] X. Ma, M.F.A. Azeez, A.F. Vakakis, Nonlinear normal modes and nonparametric system identification of nonlinear oscillators, *Mechanical Systems and Signal Processing* 14 (1) (2000) 37–48.
[19] X. Ma, A.F. Vakakis, Nonlinear transient localization and beat phenomena in a flexible system with a clearance, *Journal of Vibration and Acoustics* 123 (1) (2001) 36–44.
[20] X. Ma, A.F. Vakakis, L.A. Bergman, Proper orthogonal (Karhunen–Loeve) modes of a flexible truss: transient response reconstruction and experimental verification, *AIAA Journal* 39 (4) (2001).
[21] B.F. Feeny, R. Kappagantu, On the physical interpretation of proper orthogonal modes in vibrations, *Journal of Sound and Vibration* 211 (1998) 607–616.
[22] G. Kerschen, J.C. Golinval, Physical interpretation of the proper orthogonal modes using the singular value decomposition, *Journal of Sound and Vibration* 249 (2002) 849–865.
[23] G. Kerschen, J.C. Golinval, Nonlinear generalization of principal component analysis: from a global to a local approach, *Journal of Sound and Vibration* 254 (2002) 867–876.
[24] V. Lenaerts, G. Kerschen, J.C. Golinval, Proper orthogonal decomposition for model updating of nonlinear mechanical systems, *Mechanical Systems and Signal Processing* 15 (2001) 31–43.
[25] M.A. Trindade, C. Wolter, R. Sampaio, Karhunen–Loeve decomposition of coupled axial/bending vibrations of beams subject to impacts, *Journal of Sound and Vibration* 279 (3–5) (2005) 1015–1036.
[26] P. Glosmann, E. Kreuzer, Nonlinear system analysis with Karhunen–Loeve transform, *Nonlinear Dynamics* 41 (1–3) (2005) 111–128.
[27] W.Z. Lin, K.H. Lee, S.P. Lim, P. Lu, A model reduction method for the dynamic analysis of microelectromechanical systems, *International Journal of Nonlinear Sciences and Numerical Simulation* 2 (2) (2001) 89–100.
[28] U. Iemma, L. Morino, M. Diez, Digital holography and Karhunen–Loève decomposition for the modal analysis of two-dimensional vibrating structures, *Proceedings 10th International Congress on Sound and Vibration*, 2003.
[29] L. Sirovich, B.W. Knight, J.D. Rodrigues, Optimal low-dimensional dynamic approximation, *Quarterly of Applied Mathematics* XLVIII (3) (1990) 535–548.
[30] O. Gendelman, L.I. Manevitch, A.F. Vakakis, R. M'Closkey, Energy pumping in nonlinear mechanical oscillators: part I—dynamics of the underlying Hamiltonian systems, *Journal of Applied Mechanics* 68 (2001) 34–41.
[31] A.F. Vakakis, O. Gendelman, Energy pumping in nonlinear mechanical oscillators: part II—resonance capture, *Journal of Applied Mechanics* 68 (2001) 42–48.
[32] A.F. Vakakis, L.I. Manevitch, O. Gendelman, L. Bergman, Dynamics of linear discrete systems connected to local, essentially nonlinear attachments, *Journal of Sound and Vibration* 264 (2003) 559–577.
[33] Allen L. Edwards, *An Introduction to Linear Regression and Correlation*, W.H. Freeman and Company, San Francisco, 1976.
[34] F. Georgiades, Nonlinear Localization and Targeted Energy Transfer Phenomena in Vibrating Systems with Smooth and Non-smooth Stiffness Nonlinearities, PhD Thesis, Mechanics Division, Department of Applied Sciences, National Technical University of Athens, 2006.
[35] Young Sup Lee, Passive Broadband Targeted Energy Transfers and Control of Self-Excited Vibrations, PhD Thesis, Department of Mechanical and Industrial Engineering, University of Illinois at Urbana-Champaign, 2006.
[36] F. Nucera, Nonlinear Energy Pumping as a Strategy for Seismic Protection, PhD Thesis, Materials and Structures Engineering, University of Calabria at Arcavacata of Rende—Cosenza, 2005.
[37] R. Viguie, Passive Vibration Mitigation in Rotor Systems Using Nonlinear Energy Sinks, MSc Thesis, University of Liege, Belgium, 2005.
[38] V.I. Arnold (Ed.), *Encyclopedia of Mathematical Sciences, Dynamical Systems III*, Springer, Berlin, New York, 1988.
[39] Y.S. Lee, G. Kerschen, A.F. Vakakis, P.N. Panagopoulos, L.A. Bergman, D.M. McFarland, Complicated dynamics of a linear oscillator with a light, essentially nonlinear attachment, *Physica D* 204 (1–2) (2005) 41–69.
[40] G. Kerschen, A.F. Vakakis, Y. Sup Lee, D.M. McFarland, J. Kowtko, L.A. Bergman, Energy transfers in a system of two coupled oscillators with essential nonlinearity: 1:1 resonance manifold and transient bridging orbits, *Nonlinear Dynamics* 42 (2005) 283–303.